Supporting information

3D Printing of Self-powered Piezoelectric Sensor Enabled Gait Recognition via Deep Learning

*Xiaofei Zhang[a], Bingyu Huang[a,b], Kailong Xu[a,b], Shuzhi Sam Ge[c], Xiangxia Wei[a,]**

[a]Institute for Future (IFF), School of Automation, Shandong Key Laboratory of Industrial Control Technology, Qingdao University, Qingdao 266071, China

[b]College of Materials Science and Engineering, Qingdao University, Qingdao 266071, China

[c]Department of Electrical & Computer Engineering, National University of Singapore, 117576, Singapore.

[*]E-mail: xiangxia@qdu.edu.cn (XX Wei)

S1. The operation mechanism of the piezoelectric sensor

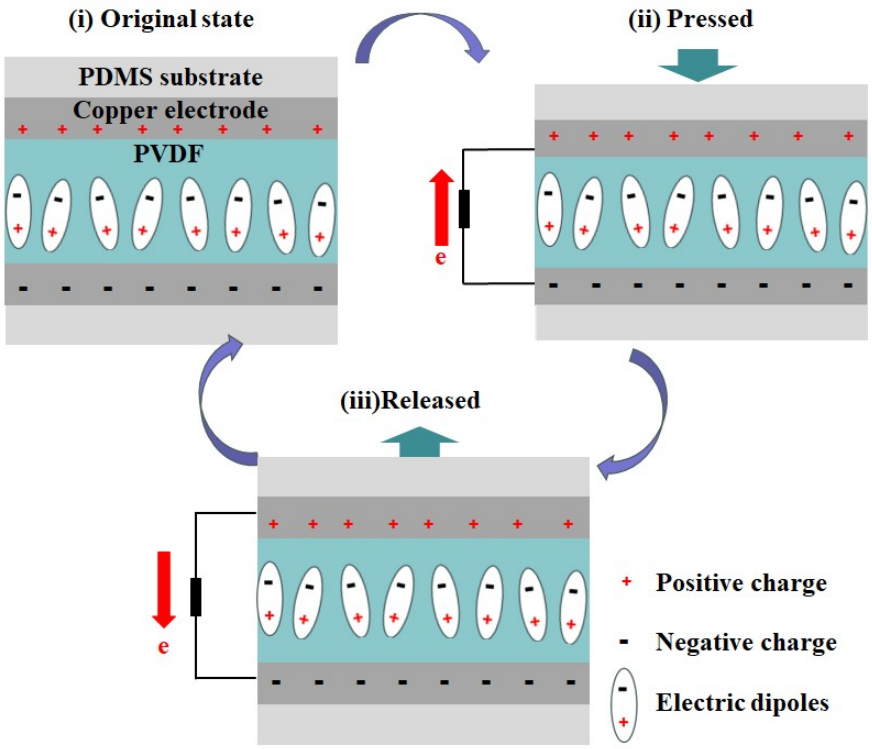

Fig. S1 The operation mechanism of the piezoelectric sensor.

S2. The piezoelectric response of PVDF fabricated via FDM and casting

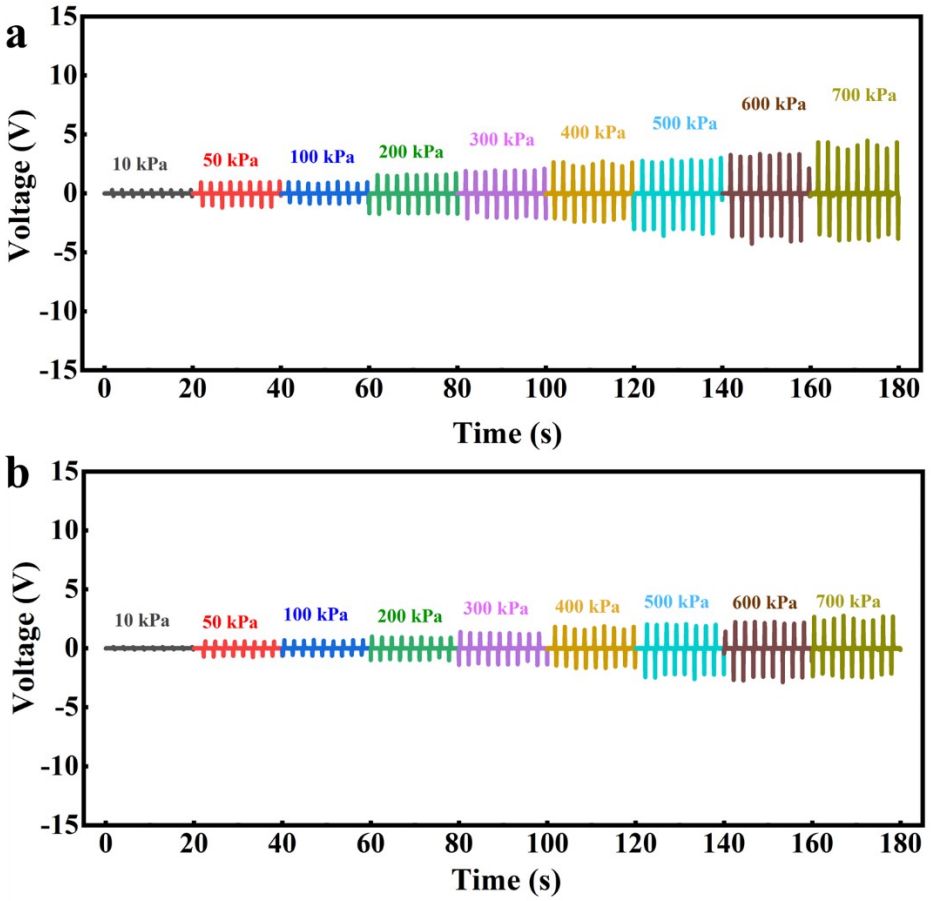

Fig. S2 Output voltage under different pressures at 1 Hz. (a) FDM printed PVDF. (b) Casted PVDF.

S3. Output performance of PVDF films with different areas

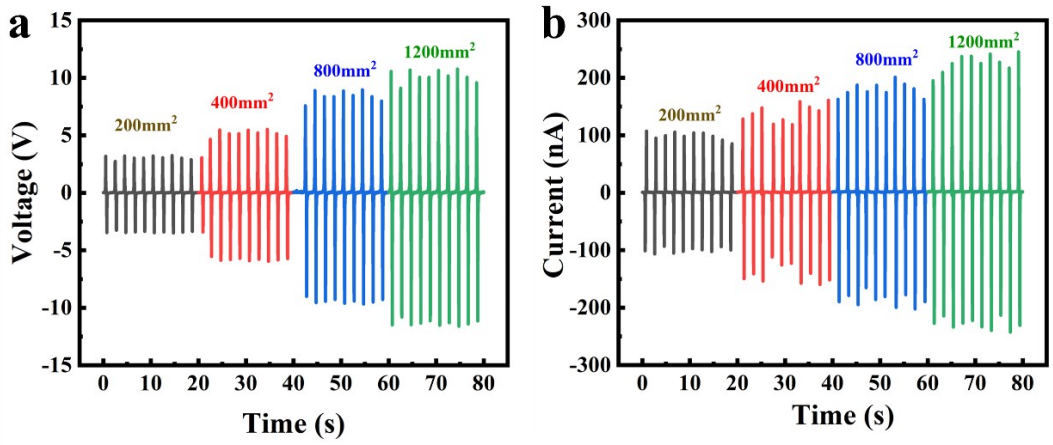

Fig. S3 Output performance of 3D printed PVDF samples with different areas at 50 kPa and 1 Hz. (a) Output voltage, (b) Output current.

S4. The piezoelectric responses with different PDMS thickness

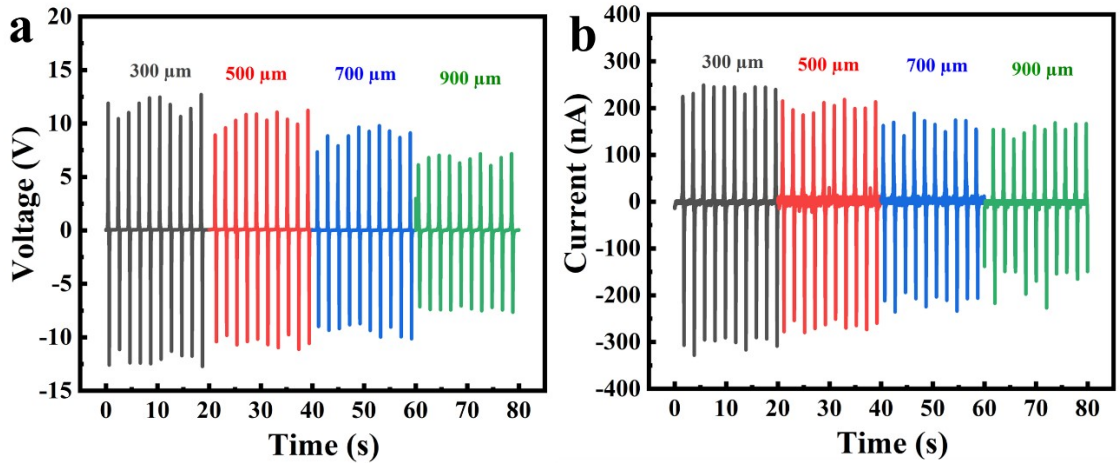

Fig. S4 The output performance of 3D-printed PVDF with different PDMS thickness. (a) Output voltage, (b) Output current.

S5. The stability of 3D-printed PVDF under different temperature and humidity

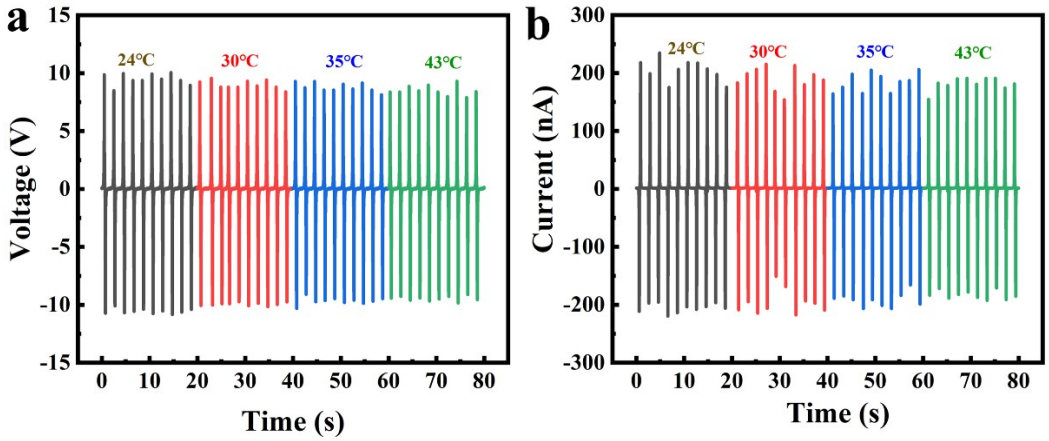

Fig. S5 The output performance of 3D-printed PVDF samples under different temperature. (a) Output voltage, (b) Output current.

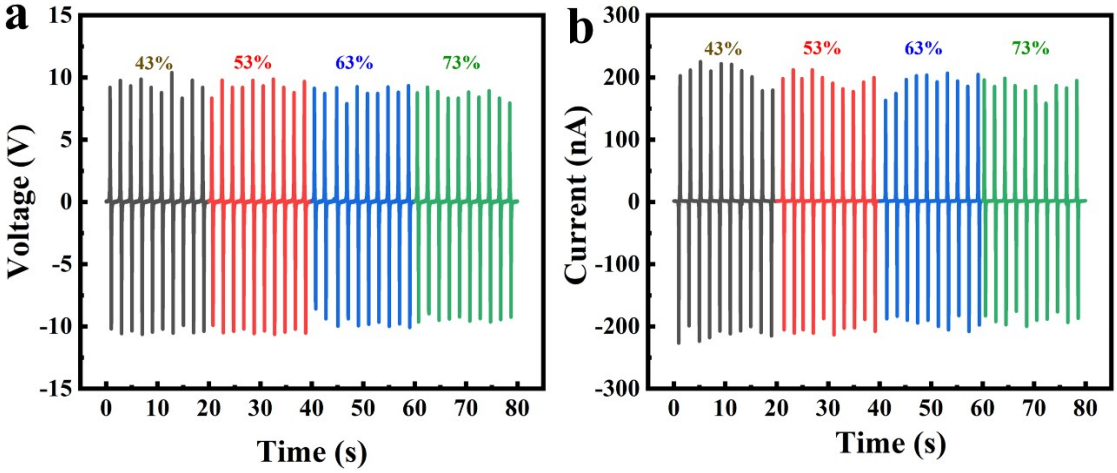

Fig. S6 The output performance of 3D-printed PVDF samples under different humidity. (a) Output voltage, (b) Output current.

S6. The change of output voltage after five months

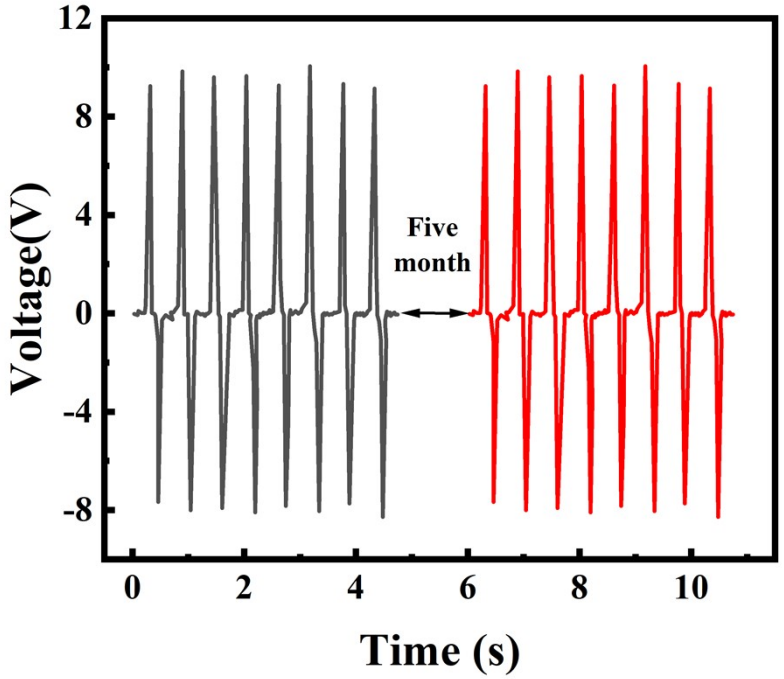

Fig. S7 The change of output voltage after five months.

S7. The intelligent system

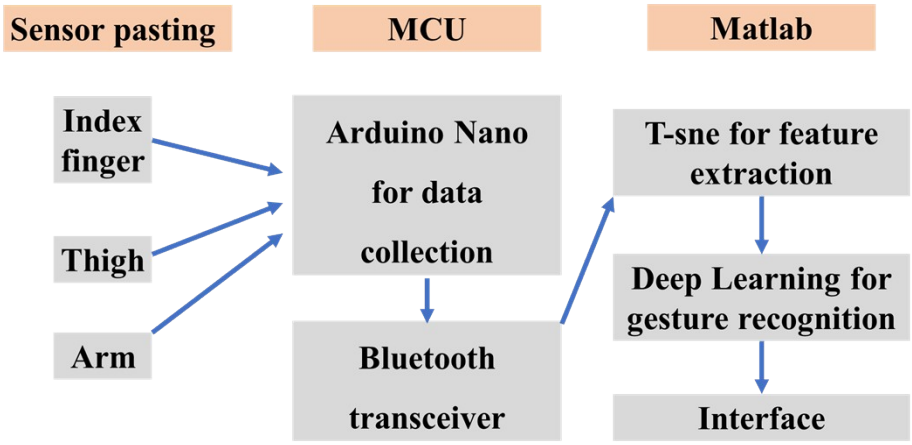

Fig. S8 The intelligent system consists of a sensor array, a printed circuit board (MCU), and a user interface.

S8. Optimization of CNN architecture parameters

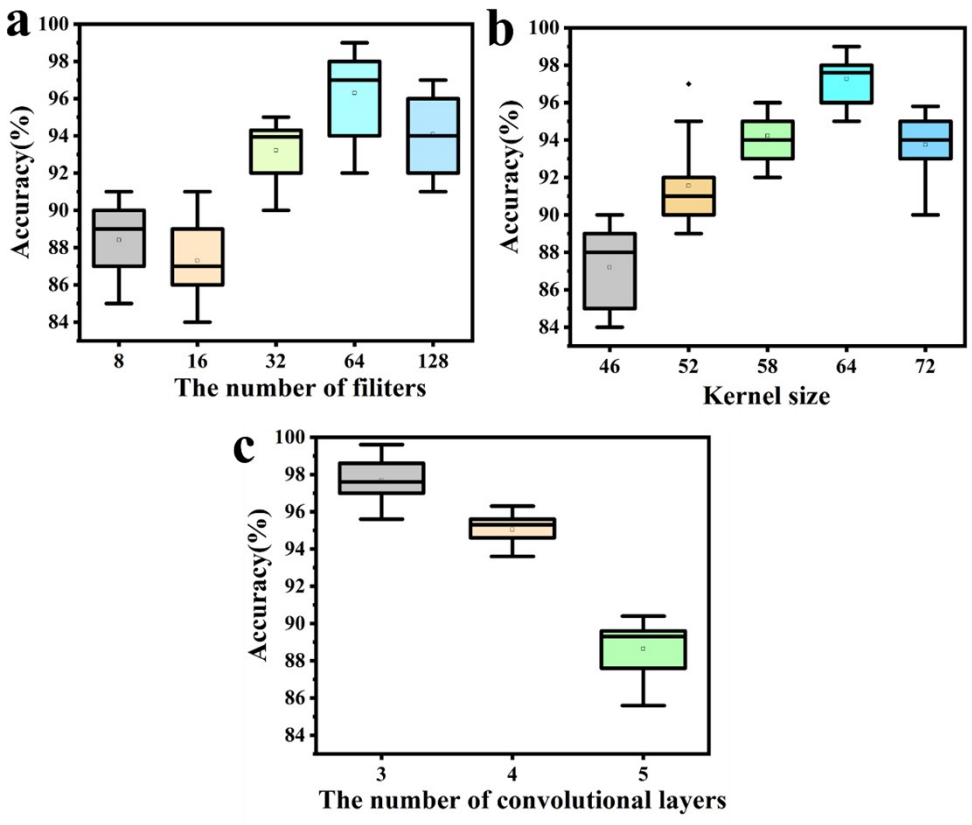

Fig. S9 Optimization of CNN architecture parameters for human posture classification.

(a) The number of filters, (b) Kernel size, (c) The number of convolutional layers.

S9. Operation process of the long short-term memory neural network unit structure

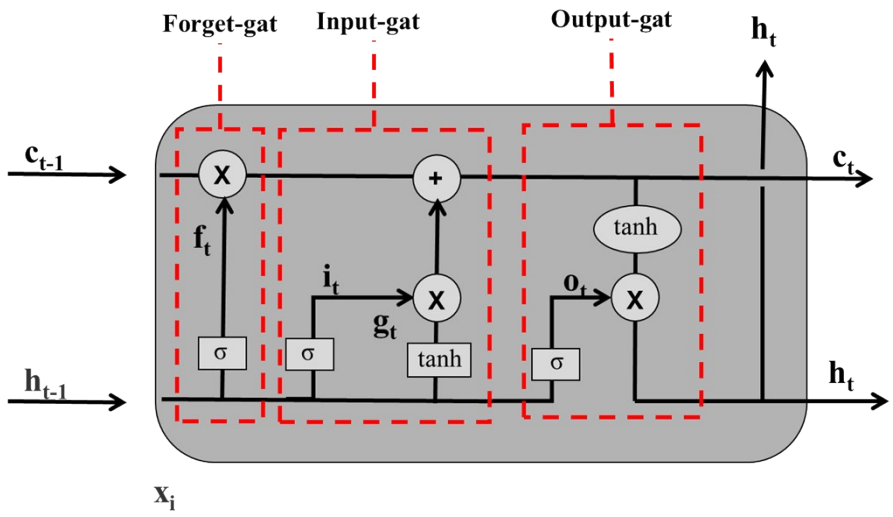

Fig. S10 Schematic diagram of long short-term memory neural network unit structure.

The LSTM unit structure shown in Figure S8. The LSTM unit structure consists of three parts: Forget-gate, Input-gate and Output-gate, which are used to select to retain or delete information.

The gate contains a Sigmoid function, which sends a value between (0,1), indicating how much input information can be transmitted. The expression of the formula is as follows:

$$\mathrm{Sigmoid}(x) = \sigma(x) = \frac{1}{1 + e^{-x}} \tag{1}$$

Forget-door: Discarding information that is no longer known or unimportant. The operation function is as follows :

$$f_t = \sigma(W_f \times [x_t, h_{t-1}] + b_f) \tag{2}$$

where, x_t is the reading of the specified time. h_{t-1} is the hidden information output by the previous structural unit. W_f is a weight matrix. b_f is a deviation

Input-gate: Determine what information is added to the cell state. The operation

function is as follows:

$$i_t = \sigma(W_i \times [x_t, h_{t-1}] + b_i \tag{3}$$

where, Wi is the Input-gate weight matrix ; bi is the Input-gate deviation ; it is output for the current moment. The tanh function is used to create a new structural unit C_t :

$$\tanh(x) = \frac{1 - e^{-x}}{1 + e^{-x}} \tag{4}$$

$$\tilde{C}_t = \tanh(W_c \times [x_t, h_{t-1}] + b_c) \tag{5}$$

$$C_t = f_t \times C_{t-1} + i_t \times \tilde{C}_t \tag{6}$$

Output-gate: Determine the useful information transmission of the current cell state. The Output-gate function expression is as follows:

$$O_t = \sigma(W_O \times [x_t, h_{t-1}] + b_O) \tag{7}$$

$$h_t = O_t \times \tanh(C_t) \tag{8}$$

The gate structural unit of long short-term memory neural network can adaptively regulate the effective information of early learning. This method solves the important events with long delay in time series.

S10. The comparison of accuracy

The main reason for choosing CNN-LSTM algorithm in gait recognition is its ability to effectively integrate spatiotemporal features. Gait is essentially a sequence with temporal continuity and spatial structure. CNN is expert in extracting spatial features of single frame images (such as joint position and limb morphology), while LSTM can capture dynamic changes across time steps in gait cycles (such as walking rhythm and motion coherence). Therefore, CNN-LSTM can adaptively learn the hierarchical expression of spatiotemporal features in gait through end-to-end joint training, which has significant advantages in dynamic behaviors modeling.

Table S1. Compare the accuracy for posture recognition by different types of sensors.

Sensor type	No. of sensors	Network type	Accuracy	Ref.
triboelectric	2	ANN	98.4%	[1]
triboelectric	5	SVM	93.1%	[2]
piezoelectric	1	LSTM	92.6%	[3]
piezoelectric	2	CNN	94.7%	[4]
piezoelectric	1	RF	96.3%	[5]
piezoelectric	2	CNN-LSTM	98.7%	This work

S11. Sensor synchronization process

To ensure accurate bilateral gait analysis, each insole-mounted sensor in our system was equipped with a MSP430F5529 microcontroller, connected via wired channels for reliable data transmission. This architecture allows motion signals to be independently collected in real time. The two microcontrollers were initialized with a shared timing reference during system startup, ensuring temporal alignment of the data streams. Key features such as speed, gait cycles, and center of mass changes were extracted from both data streams. Moreover, a specific data fusion algorithm, Kalman filtering, was then applied to combine the information into a unified signal. This design follows the principle of multi-channel signal acquisition, commonly used in glove-based or wearable systems to minimize signal interference and ensure crosstalk-free, time-aligned data fusion.

S12. The architectures and results of different models

To evaluate the robustness of our approach, we compared CNN-LSTM with other commonly used models, such as LSTM, SVM, GRU, and CNN. All models were trained and tested on the same dataset. The model parameters were listed in Table S2 and the results were summarized in Fig. S11. CNN-LSTM model consisted of two 1D convolutional layers (filters=64 and 128, kernel size=3), followed by a max-pooling layer, then connected to an LSTM layer with 100 units, and a final dense softmax output layer. LSTM algorithm is obtained by removing the original CNN layer. The GRU model consisted of a single gated recurrent unit layer with 100 units, followed by a dense softmax layer. All three models used a learning rate of 0.001, batch size of 32, and trained 100 epochs with class cross entropy loss using the Adam optimizer. Meanwhile, SVM utilized a radial basis function (RBF) kernel (C=1.0 and gamma = 'scale'), and was trained on statistical features (mean, variance, peak amplitude, step interval) extracted from the raw signals. CNN model included three 1D convolutional layers (64, 128, 128 filters), followed by ReLU activation and max pooling, then a flatten layer and a fully connected output. In summary, CNN-LSTM model outperforms others in gait classification due to its ability to extract spatial features via convolution and capture temporal dependencies through sequential modeling.

Table S2. Characteristics, parameters, and accuracy of machine learning algorithms

Model	Characteristic	Parameter	Accuracy
CNN-LSTM	Strong modeling of space and time	Conv, LSTM, Adam, 100 epochs	93.7%
LSTM	Controllable memory	LSTM, Adam, 100 epochs	90.2%
SVM	Dependent feature selection	RBF kernel, statistical features	89.9%
GRU	Gradient residue	GRU, Adam, 100 epochs	83.6%
CNN	No time modeling capability	3-layer convolution, fully connected	82.2%

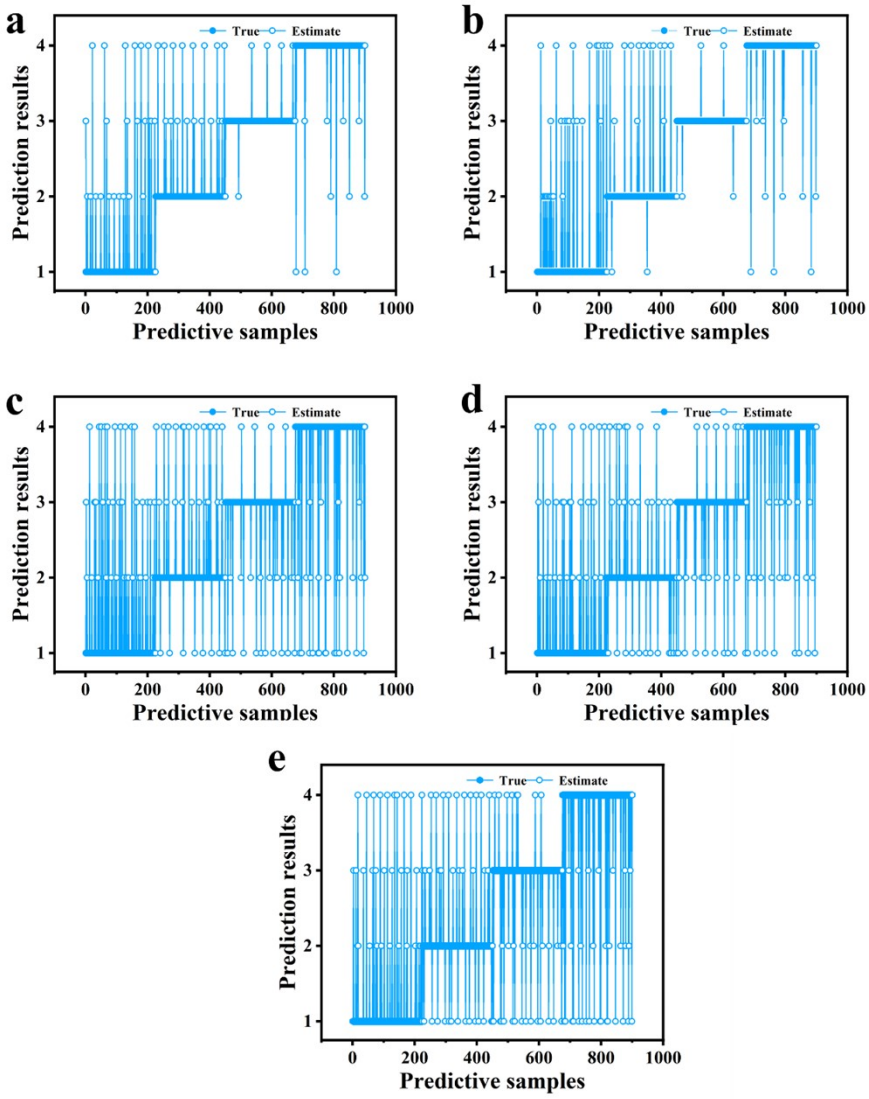

Fig. S11 Dynamic graphs for five models: (a) CNN-LSTM, (b) LSTM, (c) SVM, (d) GRU, and (e) CNN.

References

[1] Q. Zhang, T. Jin, J. Cai, L. Xu, T. He, T. Wang, Y. Tian, L. Li, Y. Peng, C. Lee, Wearable triboelectric sensors enabled gait analysis and waist motion capture for IoT-based smart healthcare applications, Adv. Sci. 9 (4) (2021) 2103694.
[2] L. Yang, W. Zihan, W. Jiyu, X. Xiao, L. Qian, D. Wenbo, H.Y. Fu, Triboelectric bending sensor based smart glove towards intuitive multi-dimensional human-machine interfaces, Nano Energy 89 (2021) 106330.
[3] Y. Guo, H. Zhang, L. Fang, Z. Wang, W. He, S. Shi, R. Zhang, J. Cheng, P. Wang, A self-powered flexible piezoelectric sensor patch for deep learning-assisted motion identification and rehabilitation training system, Nano Energy 123 (2024) 109427.
[4] G. Hao, J. Ke, Y. Fei, W. Liying, Y. Xijia, L. Xuesong, J. Yi, L. Wei, S. Xiaojuan, Multifunctional human–computer interaction system based on deep learning-assisted strain sensing array, ACS Appl. Mater. Interfaces 16(40) (2024) 54496-54507.
[5] G. Ye, Q. Wu, Y. Chen, X. Wang, Z. Xiang, J. Duan, Y. Wan, P. Yang, Bimodal coupling haptic perceptron for accurate contactless gesture perception and material identification, Adv. Fiber Mater. 6 (2024) 1874-1886.